Title

Simple and accurate expressions for diffuse reflectance of semi-infinite and two-layer absorbing and scattering media.

Journal

Applied optics, 48(35)

ISSN

1539-4522

Authors

Yudovsky, Dmitry
Pilon, Laurent

Publication Date

2009-12-10

DOI

10.1364/AO.48.006670

Peer reviewed

Simple and Accurate Expressions for Diffuse Reflectance of Semi-Infinite and Two-Layer Absorbing and Scattering Media

Dmitry Yudovsky and Laurent Pilon[§]

University of California, Los Angeles
Henry Samueli School of Engineering and Applied Science
Biomedical Engineering Inter-Departmental Program
Mechanical and Aerospace Engineering Department
Los Angeles, CA 90095-1597
[§] Corresponding Author
Phone: +1 (310)-206-5598, Fax: +1 (310)-206-4830
E-mail: pilon@seas.ucla.edu

December 15, 2010

ABSTRACT

This paper presents computationally efficient and accurate semi-empirical models of light transfer for real-time diffuse reflectance spectroscopy. The models predict the diffuse reflectance of both (i) semi-infinite homogeneous and (ii) two-layer media exposed to normal and collimated light. The two-layer medium consisted of a plane-parallel slab of finite thickness over a semi-infinite layer with identical index of refraction but different absorption and scattering properties. The model accounted for absorption and anisotropic scattering as well as for internal reflection at the medium/air interface. All media were assumed to be non-emitting, strongly forward scattering, with index of refraction between 1.0 and 1.44 and transport single scattering albedo between 0.50 and 0.99. First, simple analytical expressions for the diffuse reflectance of the semi-infinite and two-layer media considered were derived using the two-flux approximation. Then, parameters appearing in the analytical expression previously derived were instead fitted to match results from more accurate Monte Carlo simulations. A single semi-empirical parameter was sufficient to relate the diffuse reflectance to the radiative properties and thickness of the semi-infinite and two-layer media. The present model can be used for a wide range of applications including non-invasive diagnosis of biological tissue.

Keywords: diffuse reflectance, reflectance spectroscopy, Monte Carlo, turbid media, radiation properties, Kubelka-Munk theory, light dosimetry, hyperspectral imaging, skin optics

1 INTRODUCTION

Diffuse reflectance spectroscopy consists of determining the radiative properties of an absorbing and scattering sample from diffuse reflectance measurements. It has been applied to non-invasive health-monitoring of *in-vivo* biological tissues [1–7], quality control in agricultural applications [8–12], and remote terrestrial sensing [13–16], for example. In many biological applications, the irradiated medium can be modeled as a strongly scattering multilayer medium whose radiative properties are constant within each layer but differ from layer to layer. For example, the human cervix [17], colon [18], and skin [19] have been modeled as two-layer optical systems. Skin consists of an outer layer called the epidermis and of an underlying layer called the dermis. The epidermis is characterized by strong absorption in the ultraviolet and visible part of the spectrum due to melanin. On the other hand, the blood and connective tissues are responsible for absorption and scattering in the dermis. In addition, the absorption characteristics of blood depend on the concentrations of oxy- and deoxy- hemoglobin [20].

Light transfer through turbid media such as biological tissues is governed by the radiative transfer equation (RTE). The latter expresses an energy balance in a unit solid angle $\mathrm{d}\Omega$, about the direction $\hat{s}$ at location $\hat{r}$. The steady state RTE in a homogeneous, absorbing, scattering, but non-emitting medium is expressed as [21, 22],

$$\hat{s} \cdot \nabla I_\lambda(\hat{r}, \hat{s}) = -\mu_{a,\lambda} I_\lambda(\hat{r}, \hat{s}) - \mu_{s,\lambda} I_\lambda(\hat{r}, \hat{s}) + \frac{\mu_{s,\lambda}}{4\pi} \int_{4\pi} I_\lambda(\hat{r}, \hat{s}_i) \Phi_\lambda(\hat{s}_i, \hat{s}) \mathrm{d}\Omega_i \tag{1}$$

where the intensity at location $\hat{r}$ and in direction $\hat{s}$ is denoted by $I_\lambda(\hat{r}, \hat{s})$ and expressed in $\mathrm{W/cm^2 \cdot sr \cdot nm}$. The linear spectral absorption and scattering coefficients are denoted by $\mu_{a,\lambda}$ and $\mu_{s,\lambda}$, respectively and are expressed in $\mathrm{cm^{-1}}$. The scattering phase function denoted by $\Phi_\lambda(\hat{s}, \hat{s}_i)$ represents the probability that radiation propagating into the elementary solid angle $\mathrm{d}\Omega_i$ around direction $\hat{s}_i$ will be scattered in direction $\hat{\mathbf{s}}$. The first and second terms on the right-hand side of Equation (1) represent the attenuation of the radiation intensity due to absorption and out-scattering, respectively. The last term corresponds to the augmentation of radiation due to in-scattering from all directions $\hat{s}_i$ into direction $\hat{s}$. The contribution of scattering to the overall extinction is represented by the single scattering albedo ω_λ expressed as,

$$\omega_\lambda = \frac{\mu_{s,\lambda}}{\mu_{a,\lambda} + \mu_{s,\lambda}} \tag{2}$$

The Henyey-Greenstein scattering phase function is an approximate expression that accounts for the anisotropic nature of scattering and is given by [23],

$$\Phi_\lambda(\hat{s}_i, \hat{s}) = \frac{1 - g_\lambda}{(1 + g_\lambda^2 - 2 g_\lambda \cos\Theta)^{3/2}} \tag{3}$$

The Henyey-Greenstein asymmetry factor g_λ is the first moment of the scattering phase

function and is defined as [23],

$$g_\lambda = \frac{1}{4\pi}\int_{4\pi} \Phi_\lambda(\hat{s}_i, \hat{s}) \cos\Theta \mathrm{d}\Omega_i \tag{4}$$

It varies between -1 and 1. If scattering is isotropic, then the phase function is constant and g_λ equals 0. For g_λ close to -1 and 1, scattering is strongly backward or forward, respectively. The Henyey-Greenstein phase function depends only on g_λ and has been used extensively in tissue optics [4, 24, 25], computer animation [26, 27], and astronomy [28, 29], to name a few.

For the sake of clarity, the dependence of the radiative properties on wavelength will be assumed and the subscript "λ" omitted henceforth. Furthermore, all analysis and results will be presented in terms of the transport single scattering albedo ω_{tr} defined as,

$$\omega_{tr} = \frac{\mu_{s,tr}}{\mu_{s,tr} + \mu_a} = \frac{\mu_s(1-g)}{\mu_s(1-g) + \mu_a} \tag{5}$$

Here, $\mu_{s,tr} = \mu_s(1-g)$ is the transport scattering coefficient which accounts for both the magnitude and anisotropy of the scattering phenomenon [21]. For example, in case of complete forward scattering, i.e., $g = 1.00$, scattering has no effect on the propagation of light through the medium and $\mu_{s,tr} = 0.0$ [21].

The objective of this study is to develop simple and accurate expressions for the diffuse reflectance a of semi-infinite and a two-layer absorbing and scattering media. Such expressions could be combined with an inverse method to retrieve the radiation properties and thickness of these media based on spectral diffuse reflectance measurements.

2 BACKGROUND

Explicit analytical solutions of the RTE can be found only for a limited range of geometries and for simplified scattering phase functions [21,30]. Approximate or numerical solutions can be obtained based on the two-flux approximation or Monte Carlo simulations, for example.

The Two-Flux Approximation

The one-dimensional RTE can be solved by the well-known two-flux approximation [31, 32] (also called the Kubelka-Munk theory) in which the forward and backward fluxes are defined as,

$$F^+(z) = 2\pi \int_0^{\pi/2} I(z,\theta)\cos\theta\sin\theta \mathrm{d}\theta \quad \text{and} \quad F^-(z) = -2\pi \int_{\pi/2}^{\pi} I(z,\theta)\cos\theta\sin\theta \mathrm{d}\theta \tag{6}$$

where z is the depth within the medium estimated from the front surface and θ is the angle measured from the inward normal (see Figure 1). Then, the RTE simplifies to a set of two coupled linear equations [31, 32],

$$\frac{1}{S}\frac{\mathrm{d}F^+}{\mathrm{d}z} = -aF^+ + F^- \tag{7}$$

$$\frac{1}{S}\frac{\mathrm{d}F^-}{\mathrm{d}z} = -F^+ + aF^- \tag{8}$$

with $a = (S+K)/S$ where K and S are the Kubelka-Munk (K-M) absorption and scattering coefficients, respectively. They do not have any physical meaning [33] but are related to the radiative properties μ_a and $\mu_{s,tr}$ and depend on the scattering phase function.

Equations (7) and (8) have been solved for a variety of slab geometries and boundary conditions. Saunderson [34] used the two-flux approximation to predict the diffuse reflectance, denoted by $\tilde{R}_-(a)$, of a semi-infinite homogeneous medium exposed to collimated and normally incident radiation with index mismatch at the air/medium interface as [34],

$$\tilde{R}_-(a) = \rho_{01} + (1-\rho_{01})(1-\rho_{10})\frac{\tilde{R}_d(a)}{1-\rho_{10}\tilde{R}_d(a)} \tag{9}$$

where $\tilde{R}_d(a) = a - \sqrt{a^2-1}$ is the diffuse reflectance of semi-infinite medium exposed to diffuse irradiation as predicted by the two flux approximation. Note that the first term ρ_{01} corresponds to the specular reflection of incident radiation by the surrounding/medium interface while the second term accounts for the back-scattered radiation. The specular reflectivity for normally incident radiation denoted by ρ_{01} is defined as [21],

$$\rho_{01} = \left(\frac{n_1 - n_0}{n_1 + n_0}\right)^2 \tag{10}$$

The hemispherical-hemispherical reflectivity ρ_{10} is the fraction of radiation from within the medium reflected back into the medium due to index mismatch [35] and assumed to be diffusely incident upon the medium/air interface. It is given by [34–36],

$$\rho_{10} = \int_0^{\pi/2} \rho''(\theta_i)\sin 2\theta_i \mathrm{d}\theta_i \tag{11}$$

where $\rho''(\theta_i)$ is the directional specular reflectivity of the interface for angle of incidence θ_i expressed as [21],

$$\rho''(\theta_i) \;=\; \begin{cases} \frac{1}{2}\left[\frac{\sin^2(\theta_i-\theta_t)}{\sin^2(\theta_i+\theta_t)} + \frac{\tan^2(\theta_i-\theta_t)}{\tan^2(\theta_i+\theta_t)}\right] & \text{for} \quad \theta_i \le \theta_c \\ 1 & \text{for} \quad \theta_i > \theta_c \end{cases} \tag{12}$$

where θ_t is the angle of transmittance given by Snell's law (i.e., $n_0 \sin\theta_t = n_1 \sin\theta_i$) and θ_c is the critical angle defined as $\theta_c = \sin^{-1}(n_0/n_1)$ [21].

Moreover, the diffuse reflectance of a two-layer system composed of a plane-parallel slab (layer 1) of thickness L_1 over a semi-infinite layer (layer 2) exposed to collimated and normally incident irradiation has been derived as [34, 35],

$$\tilde{R}_=(a_1,a_2,Y_1) = \rho_{01} + \frac{(1-\rho_{01})(1-\rho_{10})[b_1\tilde{R}_d(a_2) + (1-a_1\tilde{R}_d(a_2))\tanh(Y_1)]}{b_1(1-\rho_{10}\tilde{R}_d(a_2)) + [a_1(\rho_{10}\tilde{R}_d(a_2)+1) - \rho_{10}^2 - \tilde{R}_d(a_2)]\tanh(Y_1)} \tag{13}$$

where $a_j = (S_j + K_j)/S_j$, $b_j = \sqrt{a_j^2 - 1}$ where subscript "j" refers to medium 1 or 2, and the K-M optical thickness is given by $Y_1 = b_1 S_1 L_1$.

If the medium is isotropically scattering then $K = 2\mu_a$ and $S = \mu_{s,tr}$ [21, 37]. However, when scattering is anisotropic, K and S depend on ω_{tr}. To find this relationship, the following approximate phase function can be used to reduce the RTE into a form that can be solved analytically [21, 22, 30, 38],

$$\Phi_\lambda(\hat{s}_i, \hat{s}) = [4g\delta(1 - \cos\Theta) + (1 - g)] \tag{14}$$

It has the same zeroth and first moments as the Henyey-Greenstein phase function [Equation (3)] which are equal to 1 and g, respectively. Van Gemert and Star [22] showed that the expression of the diffuse reflectance and transmittance found by solving the 1D RTE assuming Equation (14) has the same algebraic form as the solution developed from the two-flux approximation. Then, they developed the following relationship between the K-M absorption and scattering coefficients K and S on the one hand and μ_a and $\mu_{s,tr}$ on the other,

$$\mu_a = \eta K \quad \text{and} \quad \mu_{s,tr} = \chi S \tag{15}$$

$$\text{where,} \quad \eta = (\phi - 1)(1 - \omega_{tr})/\zeta(\phi + 1) \quad \text{and} \quad \chi = -\omega_{tr}(\phi - \phi^{-1})/(2\zeta) \tag{16}$$

The parameter ϕ is given by [22],

$$\phi = \frac{\zeta + \ln(1 - \zeta)}{\zeta - \ln(1 + \zeta)} \tag{17}$$

where ζ is the root of the characteristic equation [30],

$$\omega_{tr} = \frac{2\zeta}{\ln\left[(1 + \zeta)/(1 - \zeta)\right]} \tag{18}$$

To simplify the estimation of the diffuse reflectance, we solved Equation (18) numerically and fitted a third order polynomial to yield,

$$\zeta^2 = \frac{47}{52} + \frac{31}{49}\omega_{tr} - \frac{49}{54}\omega_{tr}^2 - \frac{17}{27}\omega_{tr}^3 \tag{19}$$

The relative difference between Equation (19) and the exact solution of Equation (18) was found to be less than 1% for $0.40 < \omega_{tr} < 1.00$. Finally, the K-M optical thickness is given by,

$$Y_1 = \zeta(\mu_a + \mu_{s,tr})L_1 = \zeta\tau_{tr,1} \tag{20}$$

where, $\tau_{tr,1} = (\mu_a + \mu_{s,tr})L_1$ is the transport optical thickness of a slab of thickness L_1 [21].

Monte Carlo Methods

Alternatively, Monte Carlo methods are commonly used to numerically solve the RTE [39–43]. To do so, a stochastic model is constructed such that the expected value of a certain random variable is equivalent to the value of physical quantity that is determined by the exact differential equation [44]. The expected value is estimated by sampling the random variable multiple times. In effect, by repeating the simulation, the variance of the estimate diminishes. Thus, the solution may be found with arbitrary accuracy by increasing the number of simulations, albeit at the cost of time [45].

Therefore, Monte Carlo simulations are difficult to use in inverse methods associated with diffuse reflectance spectroscopy [21]. Indeed, the forward problem of evaluating the diffuse reflectance must be solved numerous times to iteratively determine the medium's radiative properties. Instead, Gardner *et al.* [41] developed a semi-empirical model for one-dimensional light transfer through a semi-infinite medium exposed to collimated incident radiation based on Monte Carlo simulations. An analytical model of the fluence profile in the medium was developed using the diffusion approximation. The constants of integration, instead of being determined analytically, were found by fitting them to results from Monte Carlo simulations. The predictions of local fluence by the semi-empirical model compared well with results from Monte Carlo simulations and could be rapidly estimated.

The objective of this study is to develop a semi-empirical model for the diffuse reflectance of a non-emitting, absorbing and strongly forward scattering medium consisting of two layers exposed to collimated incident radiation. An approach similar to that used by Gardner *et al.* [41] but based on the two-flux approximation is developed in this study.

3 METHODS

Model Geometry and Radiative Properties

Figure 1 shows the one-dimensional geometries investigated in this study. First, a homoge-

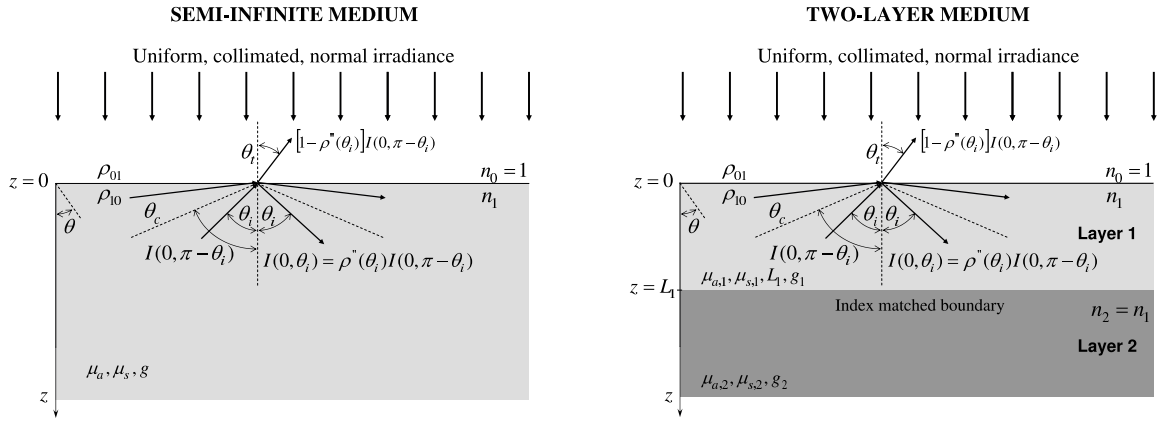

Figure 1: Schematic of the semi-infinite and two-layer media considered along with coordinate system and boundary conditions.

neous semi-infinite slab characterized by μ_a, μ_s, g, and n_1 was considered. A wide range of property values was explored namely $0.3 \leq \omega_{tr} \leq 0.99$, $0.70 \leq g \leq 0.90$, and n_1=1.00, 1.33, 1.44, 1.77, and 2.00.

Moreover, a two-layer medium was considered. It consisted of a plane-parallel slab (Layer 1) characterized by $\mu_{a,1}$, $\mu_{s,tr,1}$, g_1, n_1 and thickness L_1 supported by a semi-infinite sublayer (Layer 2) characterized by $\mu_{a,2}$ and $\mu_{s,tr,2}$, and g_2. The polar angle θ is taken relative to the inward surface normal. The physical distance from the surface is denoted by z and measured in centimeters. The thickness of Layer 1, denoted by L_1, was considered between

0 and infinity. The incident light source was modeled as a collimated, monochromatic, and normally incident beam of infinite radius and intensity $I_0 = q_0\delta(\theta)$. The quantity q_0 denotes the radiative flux of the collimated beam and $\delta(\theta)$ is the Dirac delta function. The air/slab interface and the interface between the slab and the semi-infinite sub-layer are assumed to be optically smooth. Under these conditions, radiative transfer can be considered as one-dimensional [21, 46]. Light scattering was assumed to dominate over absorption in both layers and to be strongly forward. The transport single scattering albedo of the slab $\omega_{tr,1}$ and of the sub-layer $\omega_{tr,2}$ varied between 0.50 and 0.99. The Henyey-Greenstein asymmetry factors of the two layers g_1 and g_2 varied between 0.70 and 0.90. These ranges correspond, but are not limited to, biological tissues such as the skin, muscle, and brain [4]. Finally, the index of refraction was assumed to be identical within the two layers but different from that of the surroundings. The values of refractive index investigated were $n_1 = n_2 = 1.00$, 1.33, and 1.44, corresponding to vacuum, water in the visible [47], and biological tissues in the visible and near-infrared part of the electromagnetic spectrum [4, 24]. The surrounding was assumed to be air or vacuum so that $n_0 = 1.00$.

The one-dimensional RTE given in Equation (1) was solved numerically for both geometries after specifying the boundary conditions and selecting the method of solution.

Boundary Conditions

Due to index mismatch, the collimated intensity incident onto the air/slab interface is reflected and refracted according to Fresnel's equations and Snell's law, respectively. The flux transmitted through the air/slab interface is $(1 - \rho_{01})q_0$ while the reflected flux is $\rho_{01}q_0$. In addition, light from within the slab and incident onto the slab/air interface at an oblique angle θ_i is specularly reflected with intensity $\rho''(\theta_i)I(0, \pi - \theta_i)$. On the other hand, light back-scattered from within the medium that is incident on the slab/air interface at an angle θ_i larger than the critical angle undergoes total internal reflection, as illustrated in Figure 1. Therefore, the boundary conditions of the RTE at the slab/air interface ($z = 0$) can be expressed as [21],

$$I(0, \theta) \;=\; (1 - \rho_{01})q_0\delta(\theta) + \rho''(\theta)I(0, \pi - \theta) \quad \text{for} \quad 0 \le \theta \le \pi/2 \tag{21}$$

Furthermore, the intensity vanishes as z tends to infinity, i.e.,

$$I(z \to \infty, \theta) \;=\; 0 \quad \text{for} \quad -\pi \le \theta \le \pi \tag{22}$$

Note that no reflection or refraction takes place at the slab/sub-layer interface since they have the same index of refraction. Thus, no boundary conditions need be imposed.

Method of Solution

The RTE was solved using the Monte Carlo simulation software developed by Wang and Jacques [48] for simulating light transfer through multilayer non-emitting, absorbing and scattering media. The Henyey-Greenstein scattering phase function, given by Equation (3), was used to account for anisotropic scattering. A complete and detail description of the implementation and theoretical underpinnings of this software is given in Ref. [48].

The variance in the prediction of the diffuse reflectance increases with decreasing single scattering albedo since absorption by the medium dominated over scattering resulting in fewer back-scattered photons. Thus, the number of simulated photon packets per simulation was increased until the variance associated with the estimate of the diffuse reflectance fell below 1% the most stringent case of a homogeneous medium with $\omega_{tr} = 0.50$. Each simulation required 1,000,000 photon packets or less to achieve the convergence criteria.

Diffuse Reflectance

The total intensity of the light reflected from semi-infinite or two-layer media is the sum of the specularly reflected intensity and the intensity back-scattered by the medium and transmitted through the slab/air interface. In practice, this quantity can be measured *in-vivo* by a variety of optical instruments such as an integrating sphere coupled to a detector [4]. It is denoted by $I_r(\theta_t)$ and expressed as,

$$I_r(\theta_t) \quad = \quad \rho_{01} q_0 \delta(\pi - \theta_t) + [1 - \rho''(\theta_i)] I(0, \pi - \theta_i) \quad \text{for} \quad 0 \leq \theta_i \leq \pi/2 \tag{23}$$

where θ_i is given by Snell's law. The specularly reflected intensity $\rho_{01} q_0 \delta(\pi - \theta_t)$ was ignored in this study. In practice, this is achieved by illuminating the medium with polarized light [49]. The specularly reflected intensity remains polarized and can be filtered by a linear polarizer before reaching the detector [49]. The back-scattered light is depolarized due to multiple scattering in the medium and passes unattenuated through the polarizer filter to reach the detector. Thus, the diffuse reflectance R is defined as the ratio of the back-scattered radiative flux q_r to the incident radiative flux, q_0, i.e., $R = q_r/q_0$, where q_r is expressed as,

$$q_r \quad = \quad -2\pi \int_{\pi/2}^{\pi} [1 - \rho''(\theta_t)] I(0, \pi - \theta_t) \cos\theta_t \sin\theta_t \mathrm{d}\theta_t \tag{24}$$

The goal of the study is to develop an expression to rapidly predict the diffuse reflectance of a two-layer medium as a function of its radiative and geometrical properties, namely $n_1 = n_2$, L_1, $\mu_{a,1}$, $\mu_{s,1}$, $\mu_{a,2}$, $\mu_{s,2}$, g_1, and g_2. As an intermediate step, an expression for the reflectance of a semi-infinite medium is developed.

4 ANALYSIS

Semi-Empirical Diffuse Reflectance of Semi-Infinite Media

This section aims to determine the relationship between the diffuse reflectance R_- from a semi-infinite layer and its transport single scattering albedo ω_{tr} with higher accuracy than the original two-flux approximation. Prediction accuracy was calculated relative to results from Monte Carlo simulations. Figure 2 shows the diffuse reflectance R_- as a function of ω_{tr} for $n_1 = 1.00$ for different values of g along with the predictions from the two-flux approximation given by Equations (9) and values of a obtained from Equations (15) to (17) and Equation (19). It is evident that the diffuse reflectance R_- increases with ω_{tr} as scattering dominates

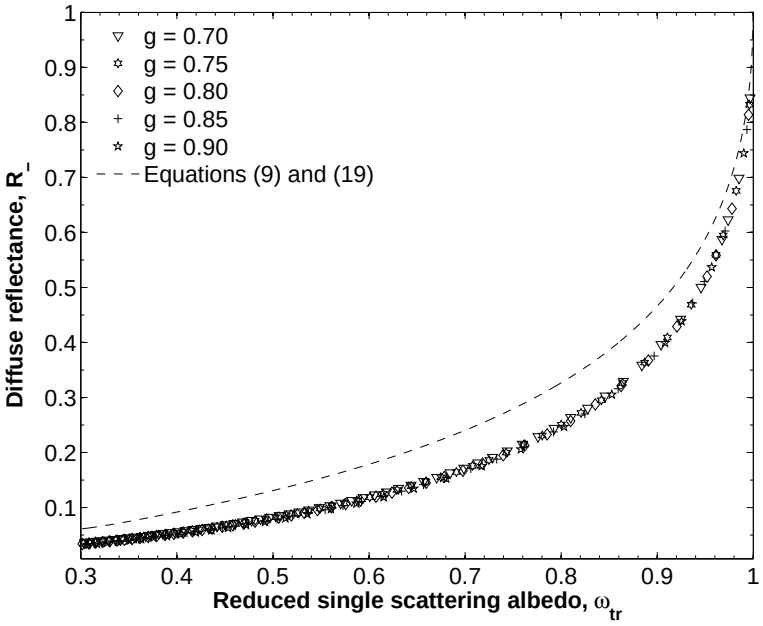

Figure 2: Diffuse reflectance of a homogeneous semi-infinite medium predicted by Monte Carlo simulations (symbols) and the two-flux approximation [Equations (9) and (19)] (dash line) for $n_1 = 1.00$, $0.3 \leq \omega_{tr} \leq 1.00$, and $0.70 \leq g \leq 0.90$.

over absorption and more light is back-scattered by the medium. Furthermore, the diffuse reflectance is almost completely determined by ω_{tr} and nearly independent of the Henyey-Greenstein asymmetry factor g in the range of interest. This is known as the similarity relation [38].

Moreover, the reflectance predicted by the two-flux approximation follows a similar trend as that predicted by Monte Carlo simulations (Figure 2). However, the relative difference varies from 100% to 5% as ω_{tr} increases from 0.3 to 1.0 for all values of g considered. This can be attributed to the fact that Equation (11) used to determine ρ_{10} was derived with the assumption that intensity at the medium/air interface was diffuse [34, 35]. Unfortunately, it is not the case [50]. Thus, unlike Monte Carlo simulations, ρ_{10} used in the two-flux approximation does not accurately account for the optical phenomena at the medium/air interface.

Consequently, Equation (9) predicting the reflectance of a semi-infinite medium was replaced by the following semi-empirical expression,

$$R_{-}(\omega_{tr}) = [1 - \rho_{01}][1 - \hat{\rho}_{10}(\omega_{tr})]\frac{\hat{R}_d(\omega_{tr})}{1 - \hat{\rho}_{10}(\omega_{tr})\hat{R}_d(\omega_{tr})} \tag{25}$$

where ρ_{01} is given by Equation (10). To account for the fact that intensity $I(z = 0, -1 \leq \mu \leq 0)$ inside the medium is not diffuse, the reflectivity ρ_{10} and the reflectance $\tilde{R}_d$ appearing in Equation (9) were respectively replaced by $\hat{\rho}_{10}$ and $\hat{R}_d$ assumed to be polynomial functions

of $a(\omega_{tr})$,

$$\hat{\rho}_{10}(\omega_{tr}) = \rho_{10} + \sum_{i=0}^{i=N} A_i [a(\omega_{tr})]^i \tag{26}$$

$$\hat{R}_d(\omega_{tr}) = \tilde{R}_d(a(\omega_{tr})) + \sum_{i=0}^{i=N} B_i [a(\omega_{tr})]^i \tag{27}$$

where $(A_i)_{0\leq i\leq N}$ and $(B_i)_{0\leq i\leq N}$ are regression coefficients and N is the polynomial order. These parameters were found by minimizing the sum of the squared residuals between the reflectance R_- obtained by Monte Carlo simulations and that predicted by Equations (25) through (27). Numerical results were found for $n_1 = 1.00$, 1.33, 1.44, 1.77, and 2.00. The polynomial order N was increased until the residual between the diffuse reflectance determined by Monte Carlo simulations and Equation (25) was small and random. This condition was met with $N = 3$. More precisely, for $0.70 \leq g \leq 0.90$, the residual was less than (i) 10% for $\omega_{tr} \geq 0.40$, (ii) 5% for $\omega_{tr} \geq 0.50$, and (iii) 2% for $\omega_{tr} \geq 0.70$.

Figure 3 shows the diffuse reflectance from a semi-infinite medium as a function of its transport single scattering albedo ω_{tr} for different values of n_1 and g. Predictions by Equations (25) through (27) are also plotted for the regression coefficients $(A_i)_{0\leq i\leq 3}$ and $(B_i)_{0\leq i\leq 3}$ reported in Table 1. The similarity relationship previously observed for the case of $n_1 = 1.00$ (Figure 2) was also valid for other values of n_1. Thus, the diffuse reflectance of a semi-infinite medium R_- is only a function of (i) the index of refraction n_1 and (ii) the transport single scattering albedo ω_{tr}.

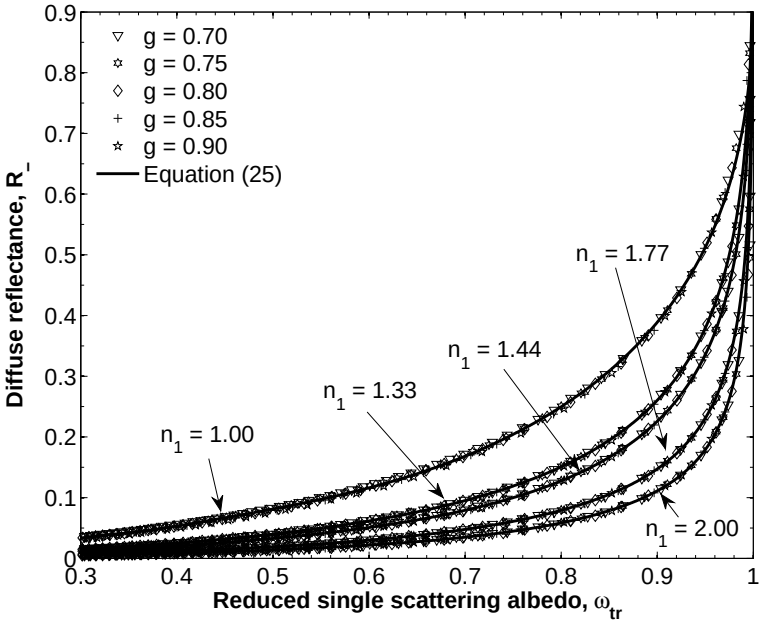

Figure 3: Diffuse reflectance of a semi-infinite homogeneous medium predicted by Monte Carlo simulations and Equations (25) for $n_1 = 1.00$, 1.33, 1.44, 1.77, and 2.00, $0.3 \leq \omega_{tr} \leq 1.0$, and $0.7 \leq g \leq 0.9$.

Table 1: Regression coefficients, $(A_i)_{0\le i\le 3}$ and $(B_i)_{0\le i\le 3}$, used in Equation (26) to estimate the diffuse reflectance R_- of a semi-infinite homogeneous medium with index of refraction $n_1 = 1.33$, 1.44, 1.77, and 2.00.

n_1	$i =$	0	1	2	3
1.00	$\mathbf{A}_i =$	0	0	0	0
	$\mathbf{B}_i =$	-6.387×10^{-2}	-1.282×10^{-2}	5.701×10^{-3}	-4.503×10^{-4}
1.33	$\mathbf{A}_i =$	-6.738×10^{-1}	1.767	-1.554	5.855×10^{-1}
	$\mathbf{B}_i =$	-9.898×10^{-2}	6.117×10^{-3}	3.774×10^{-1}	-6.291×10^{-1}
1.44	$\mathbf{A}_i =$	-6.696×10^{-1}	1.853	-1.732	6.791×10^{-1}
	$\mathbf{B}_i =$	-1.189×10^{-1}	7.524×10^{-3}	5.606×10^{-1}	-9.807×10^{-1}
1.77	$\mathbf{A}_i =$	-6.322×10^{-1}	1.716	-1.625	6.574×10^{-1}
	$\mathbf{B}_i =$	-1.192×10^{-1}	7.863×10^{-3}	7.001×10^{-1}	-1.254
2.00	$\mathbf{A}_i =$	-4.688×10^{-1}	1.234	-1.139	4.544×10^{-1}
	$\mathbf{B}_i =$	-8.223×10^{-2}	5.441×10^{-3}	6.325×10^{-1}	-1.123

Diffuse Reflectance of Two-Layer Media - Two-Flux Approximation

Figure 4a shows the diffuse reflectance of the two-layer medium $\tilde{R}_=(a_1, a_2, Y_1)$ predicted by Equation (13) as a function of the K-M optical thickness Y_1 for 9 pairs of parameters a_1 and a_2 varying between 1 and 6 while $\rho_{01} = 0.033$ and $\rho_{10} = 0.56$. These values corresponds to $\omega_{tr,1}$ and $\omega_{tr,2}$ varying between 0.50 and 1.00, $n_0 = 1.00$ and $n_1 = n_2 = 1.44$. Figure 4a shows that the diffuse reflectance of the two-layer medium progresses from $\tilde{R}_-(a_2)$ to $\tilde{R}_-(a_1)$ as Y_1 increases from 10^{-3} to 6. Indeed, there are two asymptotic cases,

$$\tilde{R}_=(a_1, a_2, Y_1) \underset{Y_1\to 0}{\longrightarrow} \tilde{R}_-(a_2) \quad \text{and} \quad \tilde{R}_=(a_1, a_2, Y_1) \underset{Y_1\to\infty}{\longrightarrow} \tilde{R}_-(a_1) \tag{28}$$

where $\tilde{R}_-(a)$ is given by Equation (9) and shown in Figure 4a. In other words, the two-layer medium behaves as a semi-infinite medium as the top layer becomes either optically thin or thick. This behavior suggests the definition of a reduced reflectance as,

$$\tilde{R}^* = \frac{\tilde{R}_=(a_1, a_2, Y_1) - \tilde{R}_-(a_2)}{\tilde{R}_-(a_1) - \tilde{R}_-(a_2)} \tag{29}$$

where $\tilde{R}^*$ increases from 0 to 1 as Y_1 varies from 0 to infinity. After combining Equations (13) and (29), the reduced reflectance can be expressed as a function of two dimensionless parameters $\tilde{\alpha}$ and Y_1,

$$\tilde{R}^*(\tilde{\alpha}, Y_1) = \frac{\tanh(Y_1)}{1/\tilde{\alpha} + (1 - 1/\tilde{\alpha})\tanh(Y_1)} \tag{30}$$

where $\tilde{\alpha}$ is given by

$$\tilde{\alpha} = 1 + \frac{\rho_{10} + \tilde{R}_d(a_2)a_1[\rho_{10}\tilde{R}_d(a_2) + 1]}{\sqrt{a_1^2 - 1}[\rho_{10}\tilde{R}_d(a_2) - 1]} \tag{31}$$

Figure 4b shows $\tilde{R}^*$ as a function of Y_1 for the same values of a_1 and a_2 used to produce Figure 4a. Unlike $\tilde{R}_=$ showed in Figure 4a, $\tilde{R}^*$ is nearly independent of a_1 and a_2. Furthermore, $\tilde{\alpha}$

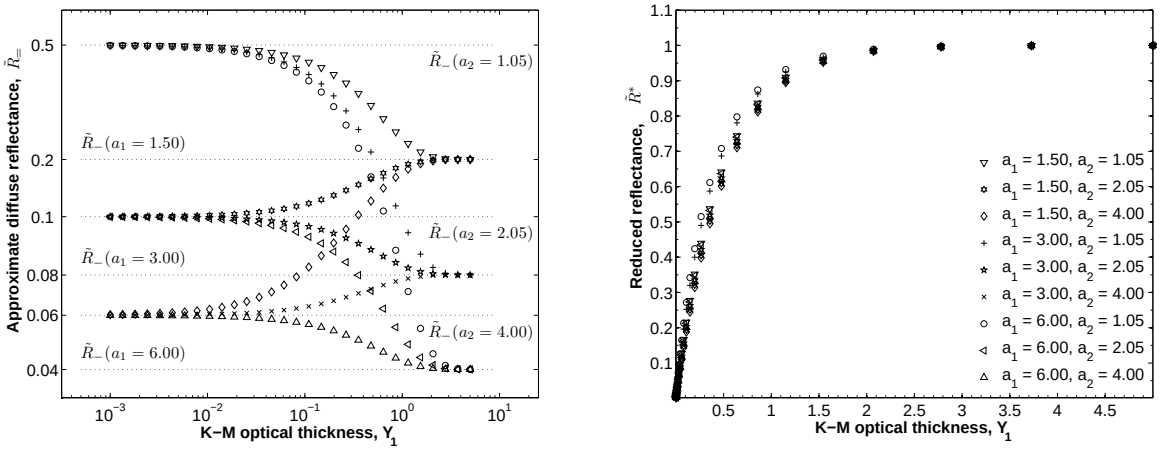

(a) (b)

Figure 4: (a) Diffuse reflectance of two-layer optical medium $\tilde{R}_=(a_1, a_2, Y_1)$ as a function of Y_1 predicted by Equation (13). Asymptotic values of $R_-(a)$ were computed from Equation (9). (b) Reduced diffuse reflectance $\tilde{R}^*$ given by Equation (29) as a function of Y_1 for different values of a_1 and a_2, $\rho_{01} = 0.033$ and $\rho_{10} = 0.56$. The legend applies to both Figures.

was found to be nearly constant and equal to 2.0 for a_1 and a_2 between 1.0 and 6.0 or $\omega_{tr,1}$ and $\omega_{tr,2}$ between 0.50 and 0.99. Similar results were obtained for other values of $n_1 = n_2$ between 1.00 and 2.00.

Diffuse Reflectance of a Two-Layer System - Semi-Empirical Expression

A semi-empirical approach similar to that presented above for a semi-infinite medium was applied to the two-layer medium described in Figure 1 to improve the accuracy of the two-flux approximation in predicting the diffuse reflectance of two-layer media. Results from Monte Carlo simulations presented in this section correspond to the case where $g_1 = g_2$. However, similar results holds for a given pair of $\omega_{tr,1}$ and $\omega_{tr,2}$ when g_1 and g_2 are different and regardless of their values between 0.7 and 0.9. This will be shown numerically in the following section.

Figures 5a and 5c show the diffuse reflectance $R_=$ of a two-layer system determined by Monte Carlo simulations as a function of Y_1 for $\omega_{tr,2} = 0.479$ and $\omega_{tr,2} = 0.958$ with $g_1 = g_2 = 0.77$, $n_1 = n_2 = 1.44$ and $\omega_{tr,1}$ ranging between 0.50 and 0.99.

The asymptotic values for smaller and larger values of Y_1 were calculated using Equations (25) through (27). The slope of $R_=(Y_1)$ was found to be positive for $\omega_{tr,1} > \omega_{tr,2}$ and negative otherwise. Furthermore, the slope of $R_=(Y_1)$ with respect to Y_1 increases as the difference between $\omega_{tr,1}$ and $\omega_{tr,2}$ increases.

Here also, a reduced reflectance R^* can be defined by analogy with $\tilde{R}^*$ given by Equation

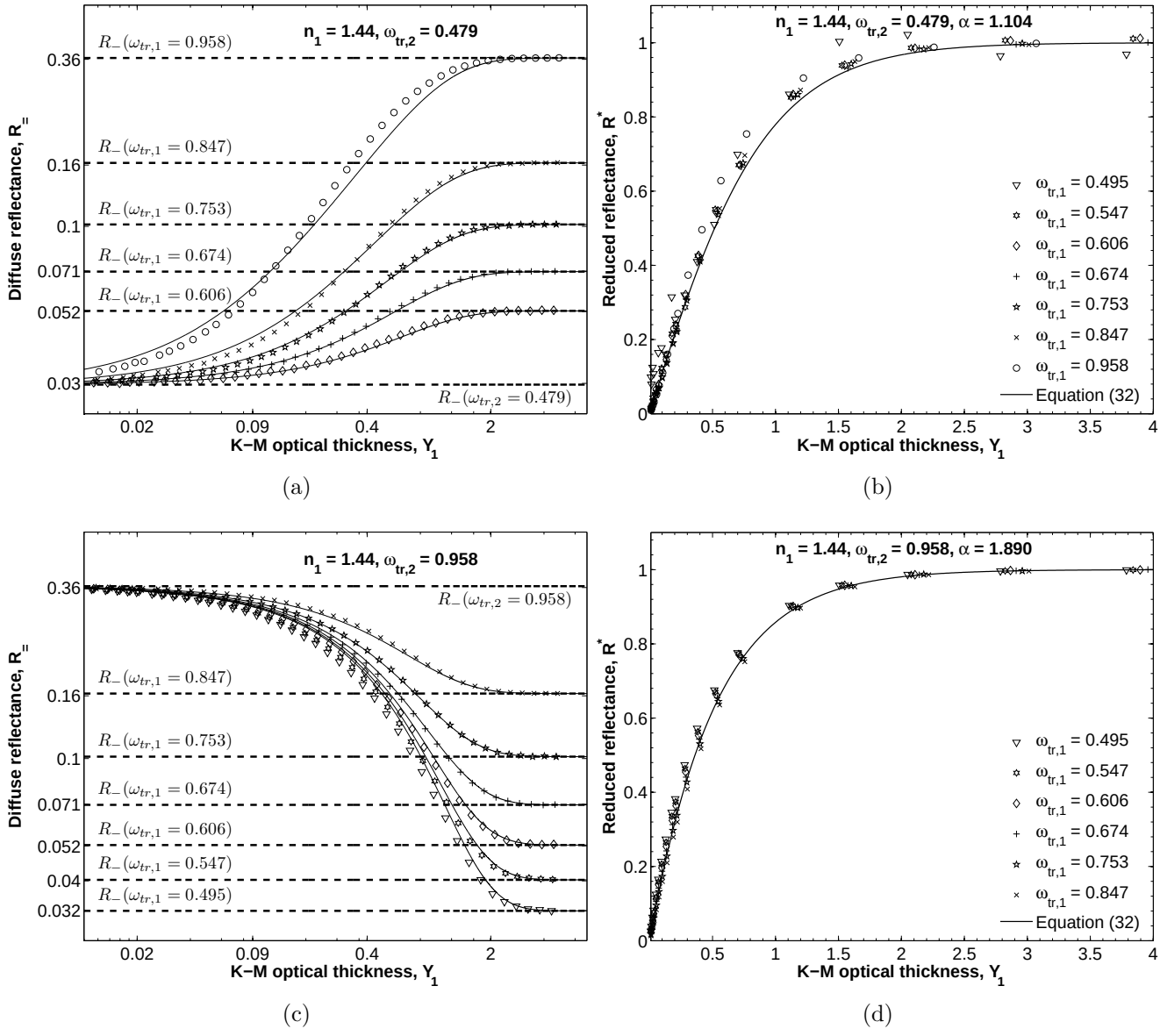

Figure 5: Diffuse reflectance $R_{=}$ predicted by Monte Carlo simulations as a function of Y_1 and corresponding reduced reflectance R^* [Equation (32)] for $n_1 = 1.44$ and (a, b) $\omega_{tr,2} = 0.479$ and (c,d) $\omega_{tr,2} = 0.958$. Predictions of $R_{=}$ by Equations (33) and (34) are also shown (solid line).

(29),

$$R^* = \frac{R_= - R_-(\omega_{tr,2})}{R_-(\omega_{tr,1}) - R_-(\omega_{tr,2})} \tag{32}$$

Note that the predictions of the single layer diffuse reflectance by the two-flux approximation $\tilde{R}_-(a_1)$ and $\tilde{R}_-(a_2)$ are replaced by the more accurate $R_-(\omega_{tr,1})$ and $R_-(\omega_{tr,2})$ predicted by Equation (25). Figures 5b and 5d show the reduced reflectance R^* as a function of Y_1 for the same parameters used to produce Figures 5a and 5b, respectively. It establishes that R^* collapses onto a single curve for $\omega_{tr,1}$ ranging between 0.50 and 0.99. In fact, no value of R^* deviates from the mean value of R^* by more than 10% for all $\omega_{tr,1}$.

The evolution of R^* differs significantly from $\tilde{R}^*$ predicted by the two-flux approximation and given by Equations (30) and (31). However, Equation (30) can be used if the parameter $\tilde{\alpha}$ is replaced by an empirical parameter α, i.e.,

$$R^* = \frac{\tanh(Y_1)}{1/\alpha + (1 - 1/\alpha)\tanh(Y_1)} \tag{33}$$

where α was found by least squares fitting of Monte Carlo simulations for R^*. A single value of α was sufficient to fit the results from Monte Carlo simulations for given values of n_1 and $\omega_{tr,2}$ and different values of $\omega_{tr,1}$ and g, i.e., $\alpha = \alpha(n_1, \omega_{tr,2})$. Predictions of the reduced reflectance R^* as a function of Y_1 by Equation (33) using $\alpha = 1.104$ are in close agreement with the more accurate Monte Carlo simulations. Thus, the diffuse reflectance of a two-layer medium can be expressed as,

$$R_= = R^*[R_-(n_1, \omega_{tr,1}) - R_-(n_1, \omega_{tr,2})] + R_-(n_1, \omega_{tr,2}) \tag{34}$$

where R_- and R^* are given by Equations (25) and (33), respectively. The reconstruction of the diffuse reflectance $R_=$ from Equation (34) agrees well with predictions from Monte Carlo simulations. The primary source of disagreement lies in the 2 to 5% relative error in $R_-(\omega_{tr,1})$ and $R_-(\omega_{tr,2})$ between Monte Carlo simulations and predictions by Equations (25) to (27) for $\omega_{tr} \leq 0.70$. For example, in Figure 5a, for $\omega_{tr,1} = 0.479$, the reduced diffuse reflectance predicted by Equations (33) deviate from Monte Carlo simulations by up to 6%. On the other hand, for $\omega_{tr,1} = 0.958$, the predictions do not deviate by more than 2%.

The above analysis was repeated for $0.50 \leq \omega_{tr,1} \leq 0.99$, $0.70 \leq g_1 = g_2 \leq 0.90$, and $0.50 \leq \omega_{tr,2} \leq 0.99$ for different values of $n_1 = n_2$. Figure 6a shows the parameter $1/\alpha$ found for $n_1 = 1.44$ and $0.70 \leq g_1 = g_2 \leq 0.90$ as a function of $\omega_{tr,2}$. It is apparent that $1/\alpha$ varies slightly with $g_1 = g_2$ and $\omega_{tr,1}$ for a given $\omega_{tr,2}$. Figure 6b shows $1/\alpha$ as a function of $\omega_{tr,2}$ for $n_1 = 1.00$, 1.33 and 1.44 and $0.70 \leq g_1 = g_2 \leq 0.90$. Also shown are the following approximate polynomial expressions for $1/\alpha$ given by,

$$1/\alpha \;\; = \;\; C(n_1)\omega_{tr,2}^2 + D(n_1)\omega_{tr,2} + E(n_1) \tag{35}$$

where C, D, and E depend on n_1 and are given in Table 2 for $n_1 = 1.00$, 1.33, and 1.44. Unlike a polynomial or other series expansion, expressing R^* by Equation (33) is well behaved in and outside the pertinent range of Y_1. It is attractive, also, because it can be estimated using the single semi-empirical parameter α. In other words, the diffuse reflectance of a two-layer medium, which, a priori, depends on eight parameters ($\mu_{a,1}$, $\mu_{s,1}$, L_1, $\mu_{a,2}$, $\mu_{s,2}$, g_1,

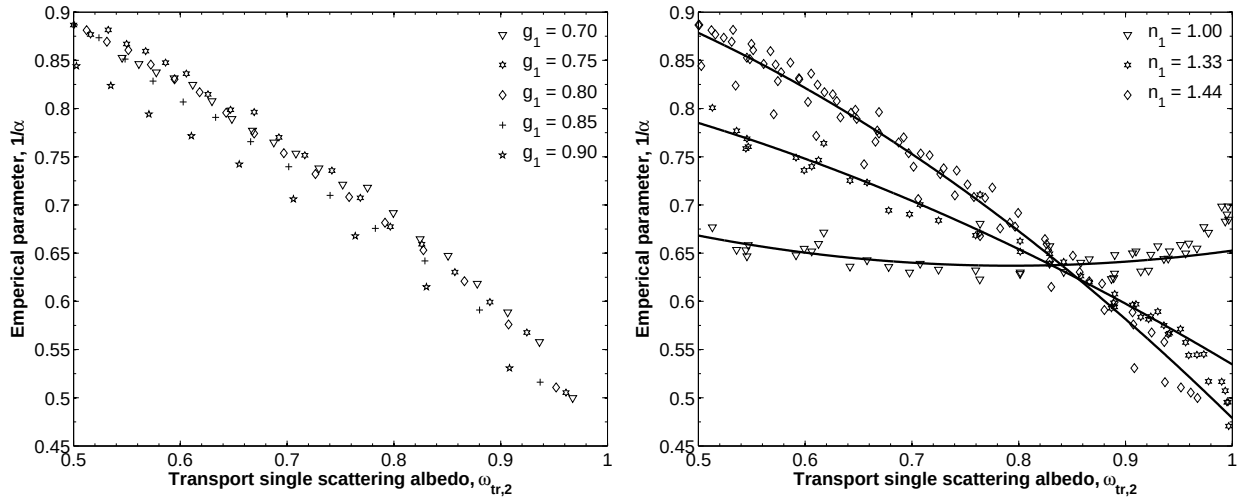

(a) (b)

Figure 6: (a) Relationship between $\omega_{tr,2}$ and $1/\alpha$ determined for $n_1 = n_2$=1.44 and $0.70 \leq g_1 = g_2 \leq 0.90$. (b) Relationship between $\omega_{tr,2}$ and $1/\alpha$ [Equation (35) and Table 2] for $n_1 = n_2 = 1.00$, 1.33 and 1.44 and $0.70 \leq g_1 = g_2 \leq 0.90$.

g_2, and $n_1 = n_2$) was reduced to a function of only three dimensionless parameters, namely (Y_1, $\omega_{tr,1}$, α). The parameter $\alpha(n_1, \omega_{tr,2})$ provides intuitive insight into the effects of the top layer on the diffuse reflectance of the two-layer medium. Differentiating Equation (33) with respect to Y_1 and setting $Y_1 = 0$ yields α, i.e., $\frac{\partial R^*}{\partial Y_1}(Y_1 = 0, \omega_{tr,1}, \omega_{tr,2}) = \alpha$. In other words, α is a measure of how effectively the top layer optically "shields" the semi-infinite layer. For larger α, $R_=$ quickly progresses from $R_-(\omega_{tr,1})$ and $R_-(\omega_{tr,2})$.

For a given $\omega_{tr,2}$, $1/\alpha$ varies with $g_1 = g_2$ up to 7% about the quadratic fits. However, the reduced diffuse reflectance R^* was found to be relatively insensitive to these variations. In fact, for the index matched case ($n_1 = n_0$), $1/\alpha$ can be treated as a constant equal to $1/\alpha = 0.656$. This results in difference in the predictions of $R_=$ by Equation (34) less than 0.1%.

Table 2: Regression coefficients in the expression of $1/\alpha$ given by Equation (35).

n_1	C	D	E
1.00	0.529	-0.759	0.831
1.33	-0.324	-0.016	0.874
1.44	-0.569	-0.055	0.993

5 RESULTS AND DISCUSSION

Comparison of Model Predictions with Monte Carlo Simulations

The accuracy of Equations (33) through (35) with values of C, D, and E from Table 2 was assessed numerically for $10^{-2} \leq Y_1 \leq 6$, $0.50 \leq \omega_{tr,1} \leq 0.99$, and $0.50 \leq \omega_{2,tr} \leq 0.99$, $0.70 \leq g_1 \leq 0.90$, $0.70 \leq g_2 \leq 0.90$ and $n_1 = 1.00$, 1.33 and 1.44 for values different from those used to generate the semi-empirical model. For Y_1 outside of the said range, the two-layer model [Equations (25), (33) and (35)] can be replaced by the single-layer model [Equation (25)]. For comparison, an additional 10,000 Monte Carlo simulations of light transfer through the two-layer medium were performed.

Figure 7a illustrates the relative error between predictions by Equation (34) and results from Monte Carlo simulations as a function of the diffuse reflectance $R_=$ for $n_1 = 1.44$, $\omega_{tr,1} \geq 0.50$, $\omega_{tr,2} \geq 0.50$ and $Y_1 \geq 0$. Similar results were obtained for different values of

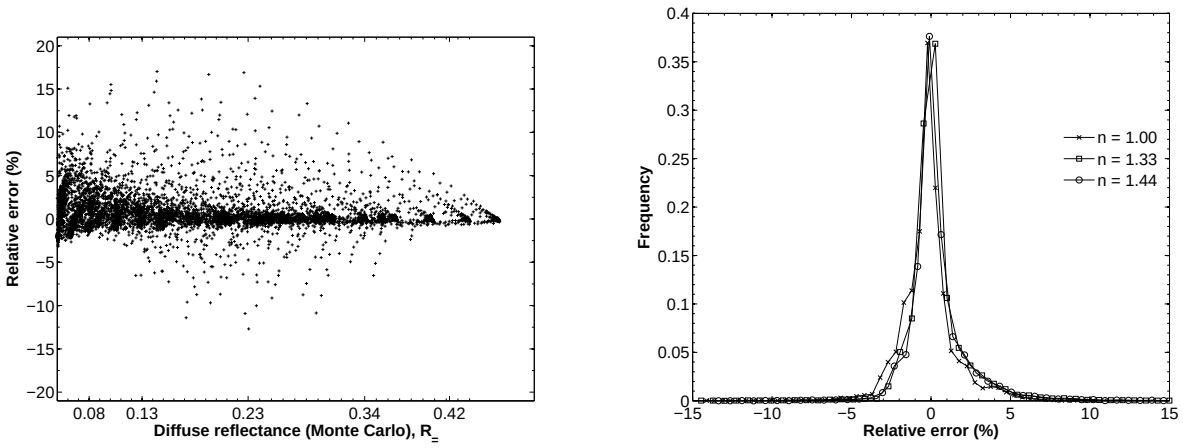

(a) (b)

Figure 7: (a) Relative error between predictions by Equation (34) and Monte Carlo simulations for $n_1 = n_2 = 1.44$. (b) Histogram of the relative error for 10,000 simulations for $n_1 = n_2 = 1.00$, 1.33, and 1.44.

n_1. The relative error ranged from -15% to 17%. It is evident that as the absolute value of $R_=$ decreases, the maximum relative error increases. Figure 7b shows the frequency of the relative error for $n_1 = 1.00$, 1.33, and 1.44. It is established that the relative error is similar for each index of refraction and less than 20%. Quantitatively, the mean and standard deviation of the relative error averaged over all n_1 are -0.16 and 1.72%, respectively. While the method performs well on average, the relative error can be larger than 10%. This is caused by two factors: (i) the inaccuracy of $1/\alpha$ [Equation (35)] in describing the two layer system and (ii) inaccuracy of Equation (25) in predicting $R_-(\omega_{tr})$. It was determined that the effects of the latter dominate over the former and that larger relative error occurs for small $\omega_{tr,1}$ and $\omega_{tr,2}$. The accuracy of Equation (25) in predicting $R_-(\omega_{tr})$ decreases for decreasing ω_{tr}. This, in turn, increases the relative error in Equation (34) since $R_=$ is a function of

R_{-}. In fact, the maximum relative error of $R_{=}$ predicted by Equation (34) compared with Monte Carlo simulations was less than (i) 17% for $0.50 < \omega_{tr,1}$ and $0.50 < \omega_{tr,2}$, (ii) 10% for $0.60 < \omega_{tr,1}$ and $\omega_{tr,2} \geq 0.60$, (iii) 4.5% for $\omega_{tr,1}$ and $\omega_{tr,2} \geq 0.75$, and (iv) 1.5% for $\omega_{tr,1}$ and $\omega_{tr,2} \geq 0.85$.

Reflectance of Human Skin

This section focuses on diffuse reflectance spectroscopy of human skin as a way to demonstrate the usefulness and accuracy of the developed model. Optical properties of skin reported in the literature are summarized before predicting the spectral diffuse reflectance between 490 and 650 nm. For these wavelengths, the epidermis and the dermis have large and significantly different absorption coefficients so that human skin behaves optically as a two layer medium. In contrast, the epidermis is essentially transparent in the near infrared and the scattering albedo approaches unity [51]. Then, the present semi-empirical model is no longer valid.

The optical properties of the human skin in the visible range depend on various biological factors and can be found in the literature [4]. The epidermis is composed mainly of dead cells, keratinocytes, melanocytes, and langerhans [40]. Melanocytes synthesize melanin, the skin protein that dominates light absorption in the epidermis (Layer 1). The absorption coefficient of the epidermis $\mu_{a,1}(\lambda)$ can be expressed as [52],

$$\mu_{a,1}(\lambda) = \mu_{a,mel} f_{mel} + (1 - f_{mel})\mu_{a,back} \tag{36}$$

where f_{mel} is the volume fraction of melanocytes in the epidermis and $\mu_{a,back}(\lambda)$ is the background absorption of human flesh given by [52, 53],

$$\mu_{a,back}(\lambda) = 7.84 \times 10^{8} \lambda^{-3.255} \tag{37}$$

Furthermore, the absorption coefficient of a single melanocytes as a function of wavelength has been approximated as [54],

$$\mu_{a,mel}(\lambda) = 6.60 \times 10^{11} \lambda^{-3.33} \tag{38}$$

Here λ is expressed in nm and $\mu_{a,back}(\lambda)$ and $\mu_{a,mel}(\lambda)$ are in cm^{-1}.

The absorption coefficient of the dermis (Layer 2) is determined primarily by the absorption of blood [55, 56] and can be written as [51, 57],

$$\mu_{a,2}(\lambda) = f_{blood}\mu_{a,blood}(\lambda) + (1 - f_{blood})\mu_{a,back}(\lambda) \tag{39}$$

where f_{blood} is the volume fraction of the dermis occupied by blood. Visible light absorption by blood is dominated by the presence of oxyhemoglobin and deoxyhemoglobin so that $\mu_{a,blood} = \mu_{a,oxy} + \mu_{a,deoxy}$. The absorption coefficient of oxyhemoglobin is given by [51, 57],

$$\mu_{a,oxy}(\lambda) = \epsilon_{oxy}(\lambda) C_{heme} SO_2 / 66,500 \tag{40}$$

where ϵ_{oxy} is the molar extinction coefficient of oxyhemoglobin [in $\text{cm}^{-1}/(\text{mole/L})$] with molecular weight of 66,500 g/mole, C_{heme} is the concentration ratio of hemoglobin in blood

[g/L], and SO_2 is the oxygen saturation defined as the mass ratio of oxyhemoglobin to total hemoglobin ($0 \leq SO_2 \leq 100\%$) [20]. Similarly, the absorption coefficient of deoxyhemoglobin is given by [51, 57],

$$\mu_{a,deoxy}(\lambda) = \epsilon_{deoxy}(\lambda) C_{heme}(1 - SO_2)/66,500 \tag{41}$$

where ϵ_{deoxy} is the molar extinction coefficient of deoxyhemoglobin. Unlike the blood volume f_{blood} and oxygen saturation SO_2 which may vary from location to location and with metabolic state, the average value of $C_{heme} = 150$ g/L is typically used [51, 58, 59]. Furthermore, the molar extinction coefficients of oxy- and deoxy- hemoglobin for a wide range of wavelengths are available in the literature [51, 60–63] and reproduced in Figure 8 in the visible range 450 to 700 nm.

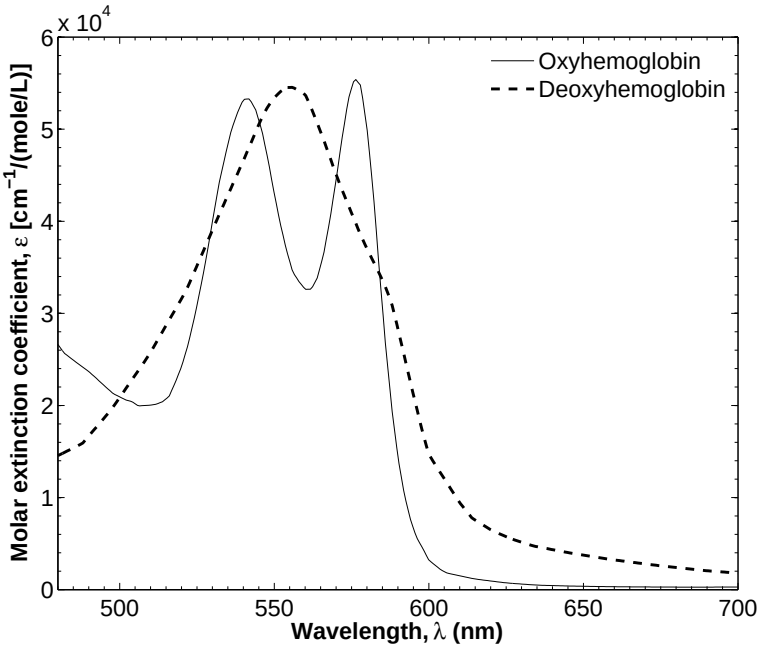

Figure 8: Spectral molar extinction coefficient of human oxy- and deoxy- hemoglobin in the visible range (480 to 700 nm) [51].

The transport scattering coefficient of biological media has been shown to follow a power law dependence on wavelength [64],

$$\mu_{s,tr} = C_{tr} \lambda^k \tag{42}$$

where λ is expressed in nm and $\mu_{s,tr}$ in cm^{-1}. For both epidermis and dermis, the values of C_{tr} and k were taken as 5.50×10^5 cm^{-1} and -1.30, respectively [65]. The thickness of the epidermis on the hand and arm ranges between 50 and 130 μm [66]. The blood volume fraction and melanocyte volume fraction range from 0.2 to 7% and from 1 to 43%, respectively [52]. In this simulation, the epidermal thickness was taken as $L_1 = 100$ μm. The epidermis and dermis were assumed to have the same index of refraction equal to 1.44 [24]. The blood volume and melanin concentrations were taken as $f_{blood} = 2.5\%$ and $f_{mel} = 1.0\%$ which are typical of healthy, lightly pigmented human skin [52].

Figure 9 shows the diffuse reflectance of human skin for $SO_2 = 0$ and 100% as predicted by Monte Carlo simulations and Equations (33) through (35) as a function of wavelength.

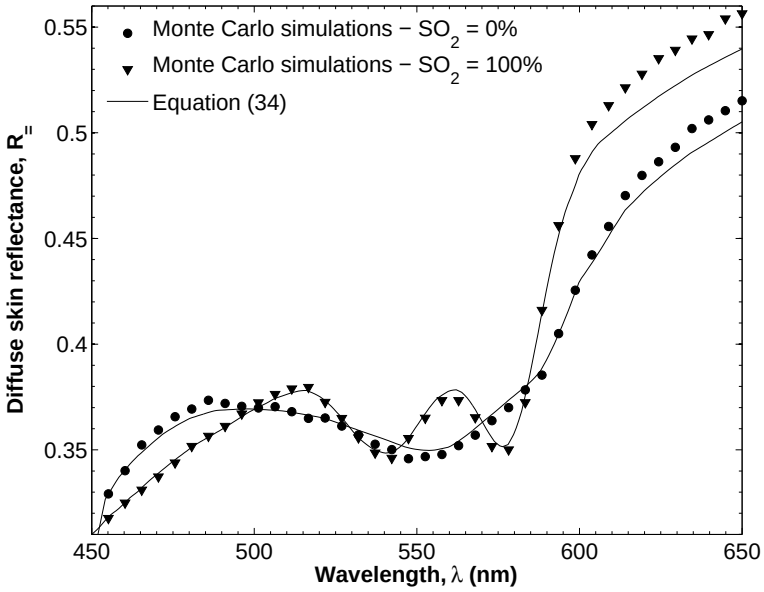

Figure 9: Comparisons of diffuse reflectance of skin predicted by Monte Carlo simulations and by Equation (34) as a function of wavelength for $f_{mel} = 1.0\%$, $f_{blood} = 2.5\%$, $L_{epi} = 100$ μm and $SO_2 = 0$ and 100%.

For high values of SO_2, i.e., for highly oxygenated blood, the skin exhibits the absorption peaks of oxyhemoglobin around 542 and 580 nm. For low SO_2, or oxygen depleted blood, the skin exhibits the single absorption peak of deoxyhemoglobin near 560 nm. In both cases, the semi-empirical model developed in this study agrees with Monte Carlo simulations within less than 8% relative error. The relative error is less than 3% for wavelength between 525 and 600 nm where absorption by oxy- and deoxy-hemoglobin is most distinct. Thus, the model can be used in diffuse reflectance spectroscopy for monitoring oxygenation and microcirculation of skin and wound.

Figure 10 shows *in-vivo* diffuse reflectance measurements from the top of the index finger of a healthy, Caucasian male subject along with a reconstruction of the same reflectance spectrum by the present model [Equations (33) through (35) and Equations (36) through (42)]. The reflectance spectrum was measured using a FDA approved hyperspectral camera (OxyVu, HyperMed Inc., Burlington MA). The reconstruction was performed by minimizing the root mean square error between the observed and reconstructed diffuse reflectance while varying f_{mel}, f_{blood}, SO_2, and L_1. The Levenberg-Marquardt algorithm [67] was used to perform the non-linear fit. The best-fit parameters found were $f_{mel} = 1.03\%$, $f_{blood} = 2.79\%$, and $SO_2 = 29.0\%$ and $L_1 = 66$ μm. The SO_2 value predicted by the present method is in close agreement with the measurement obtained with OxyVu (28%) [20]. Furthermore, the retrieved value of f_{mel} was consistent with that of Caucasian skin [52] and the estimate of f_{blood} and L_{epi} fell within the range of physiologically realistic values [52, 66]. Details discussion of the capability and robustness of inverse method using the semi-empirical model

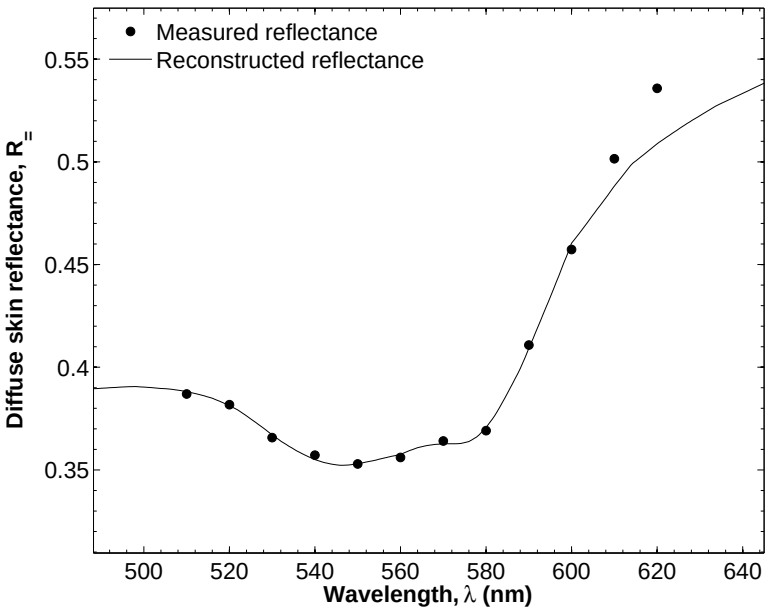

Figure 10: Experimentally measured diffuse reflectance from the top of the index finger of a healthy, Caucasian subject along with reconstructed reflectance predicted by Equations (33) through (35) and Equations (36) through (42) with best fit parameters $f_{mel} = 1.03\%$, $f_{blood} = 2.79\%$, $SO_2 = 29.0\%$ and $L_1 = 66$ μm.

developed in this paper paper and application to hyperspectral imaging of human skin will be reported in a subsequent publication.

6 CONCLUSION

A model of diffuse reflectance was developed for non-emitting, absorbing, and scattering semi-infinite and two-layer media. Scattering was assumed to be strongly forward and to dominate over absorption. First, the two-flux approximation was used to find an approximate expression for the diffuse reflectance of semi-infinite medium. Then, the coefficients of the expression were modified with numerical data from Monte Carlo simulations resulting in a semi-empirical model. Predictions from the semi-empirical model agree with results from Monte Carlo simulations within 10% for $\omega_{tr} > 0.50$. This relative error decreases to less than 2% for $\omega_{tr} > 0.70$.

Similarly, an approximate reflectance $\tilde{R}_=$ and reduced reflectance $\tilde{R}^*$ were derived from the two-flux approximation of a two-layer medium. It was shown that $\tilde{R}^*$ is a function of the two-flux optical thickness Y_1 and parameter $\tilde{\alpha}$. To account for phenomena taking place at the medium/air interface, $\tilde{\alpha}$ was replaced by an empirical parameter α which was fitted to match results from Monte Carlo simulations. Therefore, the reflectance of the two-layer medium could be expressed as a function of a single empirical parameter. The diffuse reflectance predicted by the semi-empirical model fell within 10% of results from Monte Carlo simulations for $0.60 < \omega_{tr,1}$ and $0.60 < \omega_{tr,2}$ and the different values of n_1 and τ_1 considered

in this study.

Finally, the semi-empirical model for two-layer media was applied to lightly pigmented human skin with properties taken from the literature. The model developed in this study agrees with Monte Carlo simulations within 3% relative error for wavelengths between 480 and 650 nm.

NOMENCLATURE

a, b	K-M dimensionless parameters
A_i, B_i	Single layer model fit coefficients
C, D, E	Two layer fit coefficients
C_{tr}	Scattering constant in Equation (42)
F^-, F^+	Diffuse backward and forward fluxes, W/cm^2·nm
g	Henyey-Greenstein asymmetry factor
I	Radiation intensity, W/cm^2·sr·nm
I_0	Incident radiation intensity at the slab surface, W/cm^2·sr·nm
I_r	Intensity of reflected light, W/cm^2·sr·nm
k	Scattering constant in Equation (42)
K	K-M effective absorption coefficient, 1/cm
L_1	Thickness of slab layer, cm
n_0	Index of refraction of the surrounding
$n_{1,2}$	Index of refraction of layer 1 and 2
N	Polynomial order
q_0	Radiative flux of incident beam, W/cm^2·nm
q_r	Back-scattered radiative flux, W/cm^2·nm
$\hat{r}$	Position vector, cm
R	Diffuse reflectance
R^*	Reduced reflectance
$\hat{s}$	Unit vector in a given direction
S	K-M effective scattering coefficient, 1/cm
SO_2	Oxygen saturation, %
Y	K-M optical thickness
z	Distance into the medium surface, cm

Greek symbols

α	Empirical fit coefficient of the two layer reflectance model
β	Total extinction coefficient, 1/cm
η, χ	Parameters defined by Equation (15)
θ	Polar angle, rad
θ_i	Angle of incidence on interface, rad
θ_t	Angle of transmitted radiation through interface, rad
θ_c	Critical angle for total internal reflection, rad
ϕ	Parameter defined by Equations (17)
Φ	Scattering phase function, sr^{-1}

μ	Director cosine, $\mu = \cos\theta$
μ_a	Linear absorption coefficient, 1/cm
μ_s	Linear scattering coefficient, 1/cm
$\mu_{s,tr}$	Transport scattering coefficient ($= \mu_s(1-g)$), 1/cm
ω	Single scattering albedo
ω_{tr}	Transport single scattering albedo
Ω	Solid angle, sr
ρ_{01}	Specular reflectivity to normally incident light
ρ_{10}	Hemispherical-hemispherical reflectivity
$\rho''(\theta_i)$	Directional specular reflectivity
$\tau_{tr,1}$	Transport optical thickness of the slab layer

Subscripts

1	Refers to layer 1
2	Refers to layer 2
λ	Wavelength
$=$	Refers to two-layer medium
$-$	Refers to semi-infinite medium
back	Background
deoxy	Dexyhemoglobin
d	Hemispherical-hemispherical reflectance with index matched boundary
oxy	Oxyhemoglobin

References

[1] W.M. Kuebler, "How NIR is the future in blood flow monitoring?", *Journal of Applied Physiology*, vol. 104, no. 4, pp. 905–906, 2008.

[2] A. Torricelli, D. Contini, A. Pifferi, L. Spinelli, and R. Cubeddu, "Functional brain imaging by multi-wavelength time-resolved near infrared spectroscopy", *Opto-Electronics Review*, vol. 16, no. 2, pp. 131–135, 2008.

[3] G. Zonios, A. Dimou, I. Bassukas, D. Galaris, A. Tsolakidis, and E. Kaxiras, "Melanin absorption spectroscopy: new method for noninvasive skin investigation and melanoma detection", *Journal of Biomedical Optics*, vol. 13, no. 1, pp. 014017, 2008.

[4] V.V. Tuchin, *Tissue Optics: Light Scattering Methods and Instruments for Medical Diagnosis*, Society of Photo-Optical Instrumentation Engineers, San Diego, CA, 2007.

[5] L. Khaodhiar, T. Dinh, K.T. Schomacker, S.V. Panasyuk, J.E. Freeman, R. Lew, T. Vo, A.A. Panasyuk, C. Lima, J.M. Giurini, et al., "The use of medical hyperspectral technology to evaluate microcirculatory changes in diabetic foot ulcers and to predict clinical outcomes", *Diabetes Care*, vol. 30, no. 4, pp. 903–910, 2007.

[6] R.L.P. van Veen, A. Amelink, M. Menke-Pluymers, C. van der Pol, and H. Sterenborg, "Optical biopsy of breast tissue using differential path-length spectroscopy", *Physics in Medicine and Biology*, vol. 50, no. 11, pp. 2573–2581, 2005.

[7] U. Utzinger and R.R. Richards-Kortum, "Fiber optic probes for biomedical optical spectroscopy", *Journal of Biomedical Optics*, vol. 8, no. 1, pp. 121–147, 2003.

[8] H Huang, H. Yu, H. Xu, and Y. Ying, "Near infrared spectroscopy for on/in-line monitoring of quality in foods and beverages: A review", *Journal of Food Engineering*, vol. 87, no. 3, pp. 303 – 313, 2008.

[9] A.A. Gowen, C.P. O'Donnell, P.J. Cullen, G. Downey, and J.M. Frias, "Hyperspectral imaging–an emerging process analytical tool for food quality and safety control", *Trends in Food Science & Technology*, vol. 18, no. 12, pp. 590–598, 2007.

[10] G.W. Heitschmidt, B. Park, K.C. Lawrence, W.R. Windham, and D.P. Smith, "Improved hyperspectral imaging system for fecal detection on poultry carcasses", *Transactions of the American Society of Agricultural and Biological Engineers*, vol. 50, no. 4, pp. 1427–1432, 2007.

[11] I. Kim, M.S. Kim, Y.R. Chen, and S.G. Kong, "Detection of skin tumors on chicken carcasses using hyperspectral fluorescence imaging", *Transactions of the American Society of Agricultural Engineers*, vol. 47, no. 5, pp. 1785–1792, 2004.

[12] N. Yamada and S. Fujimura, "Nondestructive measurement of chlorophyll pigment content in plant leaves from three-color reflectance and transmittance", *Applied Optics*, vol. 30, no. 27, pp. 3964–3973, 1991.

[13] M.E. Schaepman, S.L. Ustin, A.J. Plaza, T.H. Painter, J. Verrelst, and S. Liang, "Earth system science related imaging spectroscopy-An assessment", *Remote Sensing of Environment*, vol. 113, pp. 123–137, 2009.

[14] D. Landgrebe, "Hyperspectral image data analysis", *Signal Processing Magazine, IEEE*, vol. 19, no. 1, pp. 17–28, 2002.

[15] E.S. Chalhoub and H.F. Campos Velho, "Simultaneous estimation of radiation phase function and albedo in natural waters", *Journal of Quantitative Spectroscopy and Radiative Transfer*, vol. 69, no. 2, pp. 137–149, 2001.

[16] L.L. Richardson, "Remote sensing of algal bloom dynamics", *BioScience*, vol. 46, no. 7, pp. 492–501, 1996.

[17] R. Drezek, K. Sokolov, U. Utzinger, I. Boiko, A. Malpica, M. Follen, and R. Richards-Kortum, "Understanding the contributions of NADH and collagen to cervical tissue fluorescence spectra: Modeling, measurements, and implications", *Journal of Biomedical Optics*, vol. 6, no. 4, pp. 385–396, 2001.

[18] G.I. Zonios, R.M. Cothren, J.T. Arendt, Jun Wu, J. Van Dam, J.M. Crawford, R. Manoharan, and M.S. Feld, "Morphological model of human colon tissue fluorescence", *IEEE Transactions on Biomedical Engineering*, vol. 43, no. 2, pp. 113–122, 1996.

[19] S.H. Tseng, A. Grant, and A.J. Durkin, "*In-vivo* determination of skin near-infrared optical properties using diffuse optical spectroscopy", *Journal of Biomedical Optics*, vol. 13, no. 1, pp. 014016, 2008.

[20] K.J. Zuzak, M.D. Schaeberle, E.N. Lewis, and I.W. Levin, "Visible reflectance hyperspectral imaging: characterization of a noninvasive, *in-vivo* system for determining tissue perfusion", *Analytical Chemistry*, vol. 74, no. 9, pp. 2021–2028, 2002.

[21] M.F. Modest, *Radiative Heat Transfer*, Academic Press, San Diego, CA, 2^{nd} edition, 2003.

[22] M.J.C. van Gemert and W.M. Star, "Relations between the Kubelka-Munk and the transport equation models for anisotropic scattering", *Lasers in the Life Sciences*, vol. 1, no. 287–298, pp. 98, 1987.

[23] L.G. Henyey and J.L. Greenstein, "Diffuse radiation in the galaxy", vol. 93, pp. 70–83, 1940.

[24] M.J.C. Van Gemert, S.L. Jacques, H. Sterenborg, and W.M. Star, "Skin optics", *IEEE Transactions on Biomedical Engineering*, vol. 36, no. 12, pp. 1146–1154, 1989.

[25] S.L. Jacques, C.A. Alter, and S.A. Prahl, "Angular dependence of HeNe laser light scattering by human dermis", vol. 1, no. 4, pp. 309–333, 1987.

[26] K. Zhou, Z. Ren, S. Lin, H. Bao, B. Guo, and H.Y. Shum, "Real-time smoke rendering using compensated ray marching", *Association for Computing Machinery's Special Interest Group on Graphics and Interactive Techniques*, vol. 1, pp. 1–12, 2008.

[27] D.Q. Nguyen, R. Fedkiw, and H.W. Jensen, "Physically based modeling and animation of fire", in *Proceedings of the 29th Annual Conference on Computer Graphics and Interactive Techniques*. ACM New York, NY, USA, 2002, pp. 721–728.

[28] D. Calzetti, "The dust opacity of star-forming galaxies", *Publications of the Astronomical Society of the Pacific*, vol. 113, no. 790, pp. 1449–1485, 2001.

[29] JM Carvano, "Compositional interpretation of the geometric albedo of asteroids", *Astronomy and Astrophysics*, vol. 486, no. 3, pp. 1031–1038, 2008.

[30] S. Chandrasekhar, *Radiative Transfer*, Courier Dover Publications, New York, 1960.

[31] P. Kubelka and F. Munk, "A contribution to the optics of pigments", *Zeitung von Technologie und Physik*, vol. 12, pp. 593–599, 1931.

[32] A. Schuster, "Radiation through a foggy atmosphere", *The Astrophysical Journal*, vol. 21, no. 1, pp. 1–22, 1905.

[33] P. Edström, "Examination of the revised Kubelka-Munk theory: considerations of modeling strategies", *Journal of the Optical Society of America*, vol. 24, no. 2, pp. 548–556, 2007.

[34] J.L. Saunderson, "Calculation of the color of pigmented plastics", *Journal of the Optical Society of America*, vol. 32, no. 12, pp. 727–736, 1942.

[35] W.E. Vargas and G.A. Niklasson, "Applicability conditions of the Kubelka–Munk theory", *Applied Optics*, vol. 36, no. 22, pp. 5580–5586, 1997.

[36] A. Gershun, "Fresnel reflection of diffusely incident light", *Journal of the Optical Society of America*, vol. 35, no. 2, pp. 162–162, 1945.

[37] W.F. Cheong, S.A. Prahl, and A.J. Welch, "A review of the optical properties of biological tissues", *IEEE Journal of Quantum Electronics*, vol. 26, no. 12, pp. 2166–2185, 1990.

[38] G. Yoon, S.A. Prahl, and A.J. Welch, "Accuracies of the diffusion approximation and its similarity relations for laser irradiated biological media", *Applied Optics*, vol. 28, no. 12, pp. 2250–2255, 1989.

[39] S.L. Jacques, "Modeling tissue optics using Monte Carlo modeling: a tutorial", in *Optical Interactions with Tissue and Cells XIX*, S.L. Jacques, W.P. Roach, and R.J. Thomas, Eds. SPIE, San Jose, CA, USA, 2008, vol. 6854, p. 68540T.

[40] I.V. Meglinski and S.J. Matcher, "Modeling of skin reflectance spectra", 2001, vol. 4241, pp. 78–87, Society of Photographic Instrumentation Engineers.

[41] C.M. Gardner, S.L. Jacques, and A.J. Welch, "Light transport in tissue: accurate expressions for one-dimensional fluence rate and escape function based upon Monte Carlo simulation", *Lasers in Surgery and Medicine*, vol. 18, no. 2, pp. 129–138, 1996.

[42] J. Wu, F. Partovi, M.S. Field, and R.P. Rava, "Diffuse reflectance from turbid media: an analytical model of photon migration", *Applied Optics*, vol. 32, no. 7, pp. 1115–1121, 1993.

[43] H. Zeng, C.E. MacAulay, B. Palcic, and D.I. McLean, "Monte Carlo modeling of tissue autofluorescence measurement and imaging", *Advances in Laser and Light Spectroscopy to Diagnose Cancer and Other Diseases*, vol. 2135, pp. 94–104, 1994.

[44] I. Lux and L. Koblinger, *Monte Carlo Particle Transport Methods: Neutron and Photon Calculations*, vol. 650, CRC Press, Boca Raton, Florida, 1991.

[45] L. Wang, S.L. Jacques, and L. Zheng, "MCML–Monte Carlo modeling of light transport in multi-layered tissues", *Computer Methods and Programs in Biomedicine*, vol. 47, no. 2, pp. 131–146, 1995.

[46] M. Keijzer, S.L. Jacques, S.A. Prahl, and A.J. Welch, "Light distributions in artery tissue: Monte Carlo simulations for finite-diameter laser beams", *Lasers Surgery in Medicine*, vol. 9, no. 2, pp. 148–154, 1989.

[47] G.M. Hale and M.R. Querry, "Optical constants of water in the 200-nm to 200-μm wavelength region", *Applied Optics*, vol. 12, no. 3, pp. 555–563, 1973.

[48] L. Wang and S.L. Jacques, "Monte Carlo modeling of light transport in multi-layered tissues in standard C", last accessed 3/31/2009, *http://labs.seas.wustl.edu/bme/Wang/mcr5/Mcman.pdf*.

[49] S.L. Jacques, J.C. Ramella-Roman, and K. Lee, "Imaging skin pathology with polarized light", *Journal of Biomedical Optics*, vol. 7, no. 3, pp. 329–340, 2002.

[50] K.M. Katika and L. Pilon, "Steady-state directional diffuse reflectance and fluorescence of human skin", *Applied Optics*, vol. 45, no. 17, pp. 4174–4183, 2006.

[51] S. Prahl, "Optical absorption of hemoglobin", World Wide Web: http://omlc.ogi.edu/spectra/hemoglobin/hemestruct/index.html, 2002.

[52] S.L. Jacques, "Origins of tissue optical properties in the UVA, visible, and NIR regions", in *Advances in Optical Imaging and Photon Migration*, R.R. Alfano and J.G. Fujimoto, Eds., vol. 2, pp. 364–370. Optical Society of America, Washington, DC, 1996.

[53] I.S. Saidi, *Transcutaneous optical measurement of hyperbilirubinemia in neonates*, PhD thesis, Rice University, 1992.

[54] S.L. Jacques and D.J. McAuliffe, "The melanosome: threshold temperature for explosive vaporization and internal absorption coefficient during pulsed laser irradiation", *Photochemistry and Photobiology*, vol. 53, no. 6, pp. 769–775, 1991.

[55] R.R. Anderson and J.A. Parrish, "The optics of human skin", *Journal of Investigative Dermatology*, vol. 77, no. 1, pp. 13–19, 1981.

[56] M.J.C. Van Gemert, A.J. Welch, W.M. Star, M. Motamedi, and W.F. Cheong, "Tissue optics for a slab geometry in the diffusion approximation", *Lasers in Medical Science*, vol. 2, no. 4, pp. 295–302, 1987.

[57] A. Krishnaswamy and G.V.G. Baranoski, "A biophysically-based spectral model of light interaction with human skin", in *Computer Graphics Forum*. Blackwell Publishing, Inc, 2004, vol. 23, pp. 331–340.

[58] A.N. Yaroslavsky, A.V. Priezzhev, J.R.I.V. Yaroslavsky, and H. Battarbee, "Optics of blood", in *Handbook of Optical Biomedical Diagnostics*, V.V. Tuchin, Ed., pp. 169–216. SPIE Publications, Bellingham, WA, 2002.

[59] R. Flewelling, "Noninvasive optical monitoring", in *The Biomedical Engineering Handbook*, J Bronzion, Ed., pp. 1–11. IEEE Press, Boca Roton, FL, 1981.

[60] S. Wray, M. Cope, D.T. Delpy, J.S. Wyatt, and E.O. Reynolds, "Characterization of the near infrared absorption spectra of cytochrome aa3 and haemoglobin for the non-invasive monitoring of cerebral oxygenation.", *Biochimica et Biophysica Acta - Bioenergetics*, vol. 933, no. 1, pp. 184–192, 1988.

[61] A.P. Harris, M.J. Sendak, R.T. Donham, M. Thomas, and D. Duncan, "Absorption characteristics of human fetal hemoglobin at wavelengths used in pulse oximetry", *Journal of Clinical Monitoring and Computing*, vol. 4, no. 3, pp. 175–177, 1987.

[62] S Takatani and D. Graham, M, "Theoretical analysis of diffuse reflectance from a two-layer tissue model", *Biomedical Engineering, IEEE Transactions on*, vol. 26, no. 12, pp. 656–664, 1979.

[63] O.W. Van Assendelft, *Spectrophotometry of Haemoglobin Derivatives*, Thomas, Springfield, 1970.

[64] J.R. Mourant, J.P. Freyer, A.H. Hielscher, A.A. Eick, D. Shen, and T.M. Johnson, "Mechanisms of light scattering from biological cells relevant to noninvasive optical-tissue diagnostics", *Applied Optics*, vol. 37, no. 16, pp. 3586–3593, 1998.

[65] S.L. Jacques, "Skin optics", *Oregon Medical Laser Center News*, vol. 1998, no. 1, pp. 1–9, 1998.

[66] Y. Lee and K. Hwang, "Skin thickness of Korean adults", *Surgical and Radiologic Anatomy*, vol. 24, no. 3, pp. 183–189, 2002.

[67] D.W. Marquardt, "An algorithm for least-squares estimation of nonlinear parameters", *Journal of the Society for Industrial and Applied Mathematics*, vol. 11, no. 2, pp. 431–441, 1963.